Preliminary Study on Capacitive Humidity Sensors Printed on Automotive Polymer Parts

Michela Borghetti, Paolo Bellitti, Mauro Serpelloni
Department of Information Engineering
University of Brescia
Brescia, Italy
michela.borghetti@unibs.it

Abstract— **This work presents conformal capacitive humidity sensors printed directly onto non-planar polymers used in automotive components. Silver interdigitated electrodes were fabricated through Aerosol Jet Printing and photonic sintering and subsequently coated with a spray-deposited cellulose acetate butyrate (CAB) hygroscopic layer. Four representative automotive polymers, such as polyvinyl chloride (PVC), polypropylene (PP), polyethylene (PE), and PP random copolymer (PP-R), were investigated as substrates. Morphological inspection confirmed uniform line definition on all materials, while impedance analysis demonstrated a predominantly capacitive response consistent with a parallel-RC equivalent model. Controlled climatic-chamber tests at 25 °C showed substrate-dependent performance, with PP yielding the highest sensitivity and the most stable behavior across humidity steps. Dynamic cycling between 20 % and 90 % relative humidity (RH) revealed a monotonic and repeatable capacitance response, reduced hysteresis over successive cycles, and high linearity between 20 % and 70 % RH ($R^2 > 0.9921$). The PP-based sensors also exhibited excellent repeatability, with a maximum cycle-to-cycle deviation of 0.6 % at 90 % RH. These results demonstrate the feasibility and robustness of printed capacitive humidity sensors for distributed monitoring on curved automotive components, highlighting PP as a particularly suitable substrate for integration in Heating, Ventilation, and Air Conditioning (HVAC) ducts and condensation-prone surfaces.**

Keywords—humidity sensor; aerosol jet printing; interdigitated electrodes; photonic sintering; automotive HVAC; hygroscopic dielectric materials.

I. Introduction

Humidity plays a significant role in passenger comfort [1], [2], safety [3], [4], and system reliability inside road vehicles [5], [6], and its monitoring is therefore essential in several automotive subsystems. Human occupancy affects humidity levels inside the cabin, influencing thermal comfort, perceived air quality, respiratory comfort, and overall Indoor Environmental Quality (IEQ) during driving conditions [1]. In the cabin, humidity directly affects visibility, and driver alertness, since it contributes to windshield fogging [3], which remains a key safety concern for climate-control operation [7]. Beyond the cabin, humidity is also relevant near Heating, Ventilation, and Air Conditioning (HVAC) ducts, defrost channels, and window interfaces, where local vapor accumulation and condensation can impair defogging efficiency and climate-control performance [4], [8]. Modern vehicles therefore increasingly rely on humidity sensing not only to manage passenger comfort but also to guarantee optimal HVAC performance and prevent safety-critical conditions related to condensation.

While many commercial vehicles already include humidity sensors integrated into HVAC modules or intake ducts, these packaged devices provide only localized measurements and are typically constrained to planar or semi-planar mounting interfaces within the climate-control assembly. At the same time, many interior automotive components — such as door trims, pillar covers and dashboard structures — are manufactured from molded polymers with complex geometries, curved profiles, and textured surfaces. These characteristics make it challenging to integrate rigid, encapsulated humidity sensors, which generally require fixed mounting hardware and flat support surfaces, adding weight and assembly complexity while limiting design flexibility, factors that contrast with current lightweighting and modular-design objectives in automotive engineering [9].

Printed electronics offers a promising alternative for embedding sensing functionalities directly onto non-planar components. Additive manufacturing techniques enable the selective deposition of conductive traces and functional films on curved, textured, or flexible geometries, reducing or eliminating the need for separate sensor packages [10]. Several reviews highlight how printing technologies — including inkjet, screen printing, and aerosolized deposition — provide a low-cost, material-efficient route to integrating humidity, temperature, and strain sensors onto complex polymeric structures that cannot be processed using traditional microfabrication. Within this technological landscape, Aerosol Jet Printing (AJP) is particularly suitable due to its high resolution (~10 μm), compatibility with a wide range of inks, and capability of printing on non-planar and highly curved surfaces thanks to aerodynamic focusing of nanoparticle aerosols. State-of-the-art reviews describe AJP as an enabling platform for conformal printed sensors on 2.5D and 3D components—surfaces ranging from curved optical housings to structural parts where traditional deposition would be infeasible [11].

Capacitive humidity sensors are particularly well-suited to printed fabrication approaches. Their operating principle relies on monitoring changes in the permittivity of a hygroscopic dielectric, enabling stable response, low power consumption, and reduced susceptibility to leakage or contamination compared to resistive sensors [12]. A wide variety of materials has been explored for capacitive humidity detection, including synthetic polymers such as polyimide [13], poly(methyl methacrylate) (PMMA) [14], and polyvinyl alcohol (PVA) [15], as well as inorganic or hybrid dielectrics based on metal-oxide thin films [16] and sol-gel structures [17]. These families of materials offer distinct advantages: polyimide-based layers ensure good thermal stability and chemical durability; PMMA-derived films provide mechanical robustness and low-hysteresis behavior; and porous sol–gel oxides or hybrid composites can be engineered with tailored microstructures that enhance water-adsorption kinetics and improve sensitivity in the low-relative humidity (RH) regime. Both polymeric and inorganic dielectrics can reach high gravimetric and permittivity-based sensitivities when processed as thin, porous, or nanostructured films through printing or solution-based deposition [12].

This is the accepted manuscript version of the paper: 10.1109/MetroAutomotive69354.2026.11644641
© 2026 IEEE. Personal use of this material is permitted.
Permission from IEEE must be obtained for all other uses.
The final published version is available at: 10.1109/MetroAutomotive69354.2026.11644641

In parallel, cellulose-based materials have attracted substantial attention as hygroscopic dielectrics for capacitive humidity sensors, due to their natural hydrophilicity, reversible water-uptake capability, and compatibility with low-temperature deposition. Cellulose acetate, in particular, has been shown to undergo predictable humidity-induced changes in structure and dielectric properties, enabling its integration into humidity-responsive architectures and flexible devices. Building on this foundation, cellulose acetate butyrate (CAB) has demonstrated stable film-forming behavior, mechanical flexibility, and reproducible dielectric variation with absorbed moisture, supporting its adoption in both classical and more recent printed capacitive humidity-sensor designs. Blended formulations such as PVA/CAB composites can further enhance sensitivity or tailor the humidity-response curve by modifying polymer interactions and water-uptake pathways [18], [19].

Compared to these existing approaches, the present work integrates a CAB-based capacitive sensing layer directly onto non-planar automotive polymer substrates using Aerosol Jet Printing, enabling the fabrication of conformal interdigitated electrodes and uniform dielectric coatings on curved surfaces. While previous studies have focused on planar devices or flexible films, the combination of AJP patterning and spray-deposited CAB demonstrated here allows the realization of humidity sensors that can adhere seamlessly to molded polymer components commonly found inside vehicle interiors. This integration capability supports distributed humidity monitoring over complex geometries—such as door panels, pillar trims, and dashboard structures—where commercial packaged sensors cannot be mounted, and where localized condensation or moisture ingress may occur but remain undetected by traditional point-based sensing approaches.

II. HUMIDITY SENSORS FABRICATION

A. *Materials and Design*

Four commercially available polymer tubes were selected as substrates for the fabrication of the conformal humidity sensors: a light-gray polyvinyl chloride (PVC) tube with an outer diameter of 25 mm and a wall thickness of 3 mm, a gray polypropylene (PP) tube with a 32 mm outer diameter and 2 mm wall thickness, a black polyethylene (PE) with a 32 mm outer diameter and 3 mm wall thickness, and a green PP random copolymer (PP-R) tube having a 20 mm outer diameter and 3.4 mm wall thickness. Each pipe was cut into 7-cm-long samples to provide a proper surface region for sensor deposition. Silver interdigitated electrodes (IDEs) were fabricated using a silver nanoparticle ink (GenesInk SmartAero), specifically formulated for aerosol jet printing. This ink provides high adhesion to polymeric substrates and maintains mechanical compliance after deposition. Its formulation also enables efficient photonic sintering, allowing the formation of a conductive metallic network while avoiding excessive thermal exposure to the underlying polymers. Electrical contacts were realized by bonding 24-AWG copper wires to the printed pads using a silver-filled conductive epoxy (Chemtronics CW2400), ensuring mechanically robust and low-resistance interconnections. As dielectric material, cellulose acetate butyrate (CAB, CAS 9004-36-8) was employed. A 1 wt% CAB solution in acetone was prepared by magnetic stirring at room temperature until complete dissolution. This concentration was selected to obtain a solution suitable for spray deposition, ensuring adequate wettability, uniform film formation, and conformal coverage of the curved tube surfaces.

The sensing structure consists of a capacitive IDE geometry (Fig. 1), whose impedance varies with ambient humidity due to modulation of the dielectric properties of the overlying hygroscopic layer. The active area corresponds to a region of 10.3 mm × 5.25 mm. The dimensions were intentionally designed to yield a baseline capacitance exceeding 1 pF, ensuring a robust signal-to-noise ratio, while keeping the sensing footprint sufficiently small to support comparative studies across different substrates and potential implementation on a variety of curved or space-constrained components. The IDE geometry was kept identical for all substrates to isolate the effect of the underlying polymer on the sensor response and avoid geometry-dependent bias in the comparison. The extremely low consumption of ink and dielectric material results in an estimated material cost of only a few tens of euro cents per sensor.

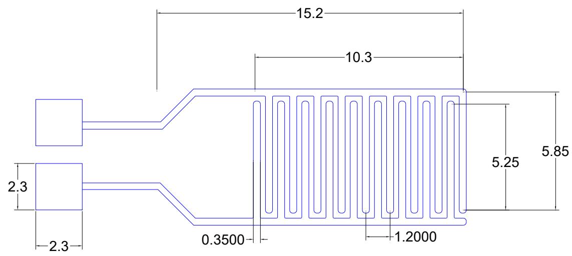

Fig. 1. Schematic representation of the IDE geometry with main dimensions (in mm).

B. *Fabrication Method*

Fig. 2 illustrates the main steps of the fabrication process. Prior to printing, the tube surfaces were cleaned with isopropyl alcohol and dried with compressed air.

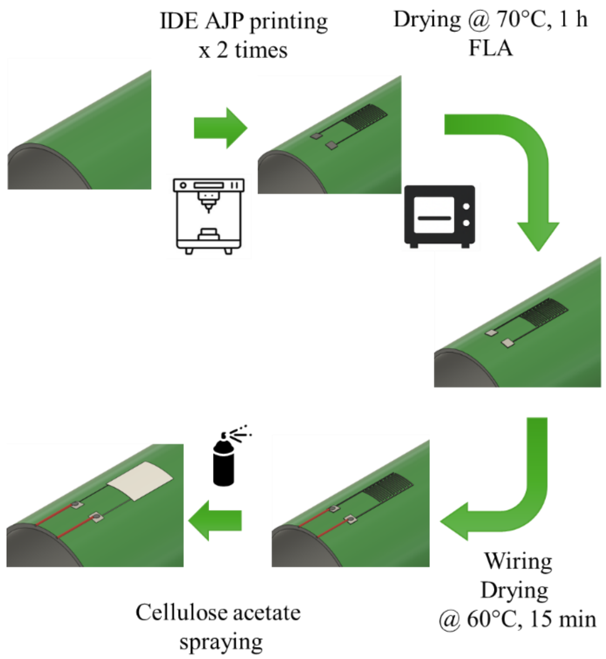

Fig. 2. Schematic representation of the fabrication process for the printed humidity sensor on a polymeric pipe.

The AJP system (Optomec AJ-300) was programmed using a CAD layout of the IDE geometry. The silver ink was atomized in a nitrogen carrier stream and focused through a nitrogen sheath flow. Printing was performed with a 750 µm nozzle (the effective linewidth is determined by aerodynamic focusing of the aerosol stream by the sheath gas rather than by the nozzle diameter, allowing features much smaller than the nominal nozzle size to be deposited) at a speed of 2 mm/s and a nozzle-to-surface distance of 4 mm. Owing to the cylindrical shape of the tubes, the printer maintained a constant standoff distance along the entire pattern. Process parameters were optimized to achieve uniform line definition, with linewidths of approximately 0.35 mm. Each pattern was printed twice to increase trace thickness and reduce electrical resistance. Solvent evaporation was carried out in a static oven at 70 °C for 1 h. The tubes were then transferred to a photonic curing system (PulseForge 1300, NovaCentrix), where high-energy light pulses were applied to sinter the metallic ink. The selected pulse profile enabled efficient curing while avoiding thermal deformation of the polymeric tubes. Electrical leads were attached via silver-filled epoxy cured at room temperature. Finally, the CAB solution was spray-coated onto the printed IDEs to form the hygroscopic dielectric layer. Representative printed sensors on PP-R, PVC, PP, and PE substrates are shown in Fig. 3.

C. Morphological and Electrical Analysis

The morphology of the printed silver traces was examined using an optical microscope (Orma Scientific) operating at 2× magnification and equipped with a USB digital camera. This inspection, performed prior to the deposition of the cellulose-acetate-butyrate (CAB) layer, enabled verification of line continuity, uniformity, and lateral spreading on the curved polymer surfaces. Across all substrates (PVC, PP, PE, and PP-R), the printed linewidth was measured as (0.36 ± 0.02) mm, consistent with typical Aerosol Jet Printing tolerances, which are generally between 10 % to 15 % of the nominal feature size. Fig. 4 provides a representative microscopic image of the IDE pattern printed on the PP tube, illustrating the good edge definition and continuity of the deposited features.

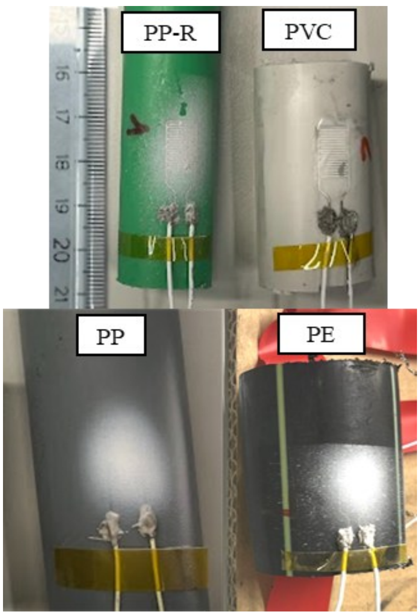

Fig. 3. Photographs of the four tubes made of PP, PE, PVC, and PP-R, each equipped with a printed humidity sensor.

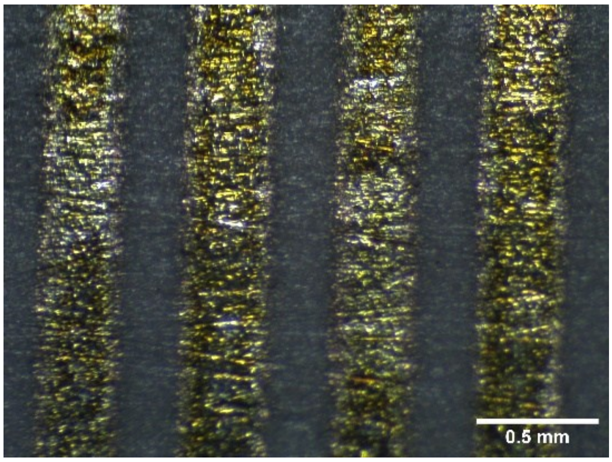

Fig. 4. Photograph at the microscope of a portion of the humidity sensor on PP.

Electrical characterization was then performed to assess the baseline impedance response and validate the expected equivalent circuit. A Keysight E4990A impedance analyzer was used to acquire complex impedance spectra in the 1 kHz – 1 MHz range, with 1601 logarithmically spaced sampling points, under ambient laboratory conditions (approximately 50 % RH). The impedance magnitude exhibited an approximately −20 dB/decade slope, while the phase remained close to −90°, confirming that the devices behave predominantly as capacitive elements and follow a parallel-RC model consisting of a geometric capacitance Cp and a leakage resistance Rp.

The effect of the CAB hygroscopic dielectric was assessed by comparing devices before and after the coating. The Bode magnitude and phase diagrams of the sensors on PP tube with and without the CAB coating are shown in Fig. 5 and Fig. 6, clearly showing that the RC-like behavior is preserved after deposition of the hygroscopic dielectric layer. Bare IDE structures exhibited capacitances from 1.9 pF to 2.1 pF, depending on the substrate. After deposition of the CAB dielectric layer, the extracted equivalent capacitance Cp showed substrate-dependent variations. The measured capacitance was approximately 2.98 pF on the PVC tube, 2.73 pF on the PP tube, 2.68 pF on the PE tube, and 2.41 pF on the PP-R tube.

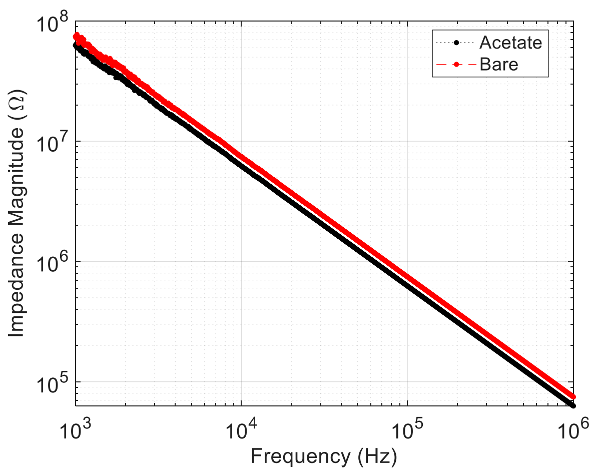

Fig. 5. Impedance magnitude of the PP-based capacitive humidity sensor, comparing the device after deposition of the cellulose acetate dielectric layer and the bare IDE structure.

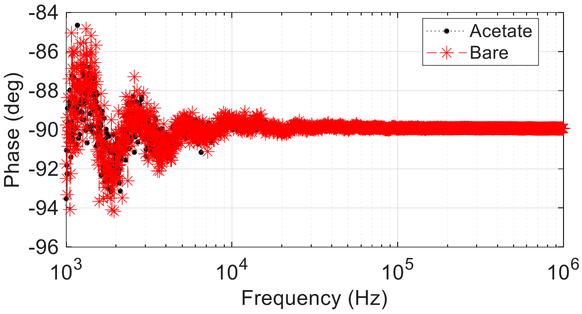

Fig. 6. Phase response of the PP-based capacitive humidity sensor, comparing the device after deposition of the cellulose acetate dielectric layer and the bare IDE structure.

These differences arise from the distinct dielectric properties and surface characteristics of the underlying polymers, which modulate the electric-field distribution beneath the IDEs. The leakage resistance remained above 1 GΩ for all substrates, indicating negligible conductive paths and confirming the predominance of the capacitive behavior. This preliminary electrical assessment demonstrates that all printed sensors exhibit stable capacitive characteristics and adhere to the parallel-RC model, establishing a consistent baseline for the controlled humidity measurements described in Section III.

III. Experimental Setup

The humidity-controlled characterization was performed inside a Compact Benchtop Climatic Chamber DY200 C (Angelantoni Test Technologies). Throughout all experiments, the chamber maintained a stable temperature of 25 ± 1 °C, while both temperature and RH were continuously recorded every 10 s by internal sensors and saved. These environmental data were later synchronized with the electrical data acquired by the impedance analyzer, enabling direct time-domain correlation between the imposed climatic conditions and the sensor response.

Two humidity-profiling procedures were implemented.

In the first procedure, referred to as Test #1, a single representative sample for each of the four substrates (PE, PP, PP-R, and PVC) was evaluated inside the chamber, under an identical humidity profile. During this test, the chamber RH was sequentially set to 20 %, 50 %, and 80 %, and then decreased again to 50 % and 20 %, with each level held for 1000 s. The impedance of the devices was monitored using a Keysight E4990A impedance analyzer connected to a laptop that handled the data-logging operations. The impedance analyzer performed repeated frequency sweeps in the 1 kHz – 1 MHz range, using 200 logarithmically spaced points, with one complete spectrum acquired every 60 s. These spectra were both to examine the stability of the sensor response across the humidity transitions and to extract the equivalent capacitance Cp at multiple frequencies. This analysis enabled the identification of the most suitable operating frequency based on sensitivity, stability, and susceptibility to low-frequency dispersion.

Since the sensors printed on PP exhibited the most stable and low-noise behavior, the second procedure, Test #2, was performed exclusively on PP samples. In this protocol, the RH was increased from approximately 20 % to 90 % in 10 % increments, with each level maintained for 20 min, and then decreased following the same sequence. This upward–downward cycle was repeated three times. For this test, the primary variable was the equivalent capacitance Cp extracted at 20 kHz, sampled at 13 kS/s offering high-resolution temporal tracking of the capacitance evolution.

IV. Results and Discussion

Fig. 7 shows the relative humidity profile imposed by the climatic chamber during Test #1, together with the corresponding measured RH. The chamber accurately tracks the programmed humidity levels, although small transients appear at each transition. The figure also shows the temperature setpoint and the temperature measured by the chamber sensors, both of which remain confined within a narrow band around the nominal 25 ± 1 °C condition.

The impedance behavior of the sensor fabricated on PP, selected as a representative case among the three substrates, is reported in Fig. 8 and Fig. 9 in terms of its equivalent capacitance Cp and parallel leakage resistance Rp, respectively.

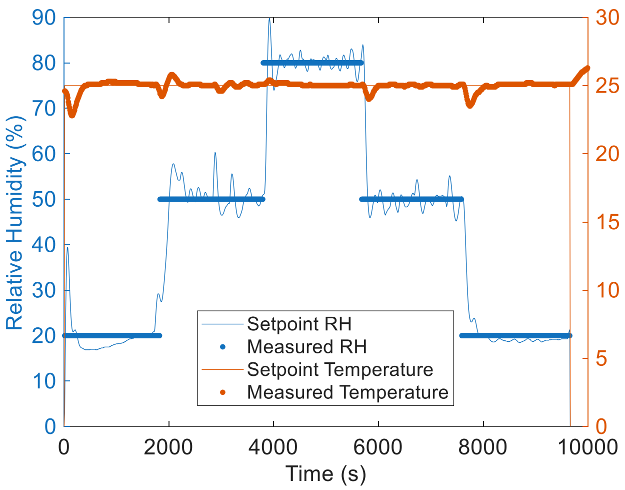

Fig. 7. Relative humidity (RH) profile during Test #1, showing the RH setpoint imposed by the climatic chamber (thick blue line) and the corresponding measured RH values (blue line), as well as the temperature setpoint imposed by the climatic chamber (thick red line) and the corresponding measured temperature values (red line).

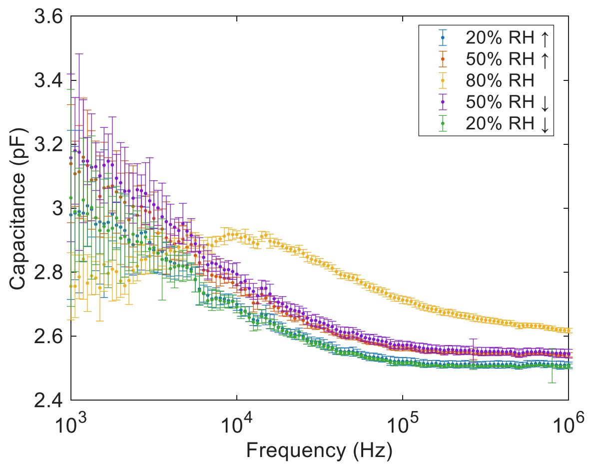

Fig. 8. Equivalent capacitance (Cp) extracted from impedance spectra of the PP-based sensor during Test #1.

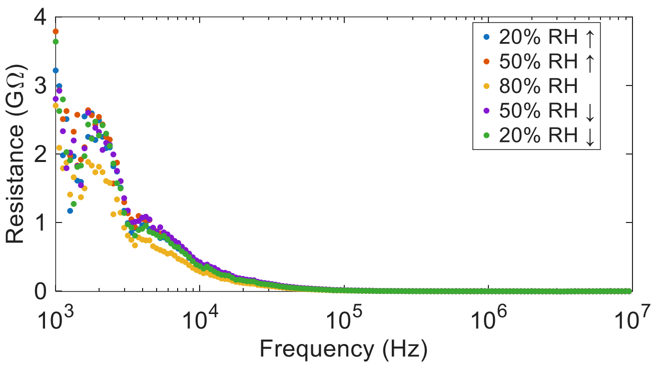

Fig. 9. Equivalent capacitance (Rp) extracted from impedance spectra of the PP-based sensor during Test #1.

Analysis of Cp across frequencies reveals that the lowest frequencies (< 7 kHz) exhibit an inconsistent trend at 80 % RH, where the capacitance unexpectedly decreases instead of increasing. This effect is attributed to low-frequency dispersion and parasitic contributions that distort the capacitive response. Above this region, the device follows the expected monotonic behavior. The highest sensitivity is observed between 20 kHz and 34 kHz, where the capacitance increases consistently with RH. Among these, 20 kHz provides the best trade-off between sensitivity and stability, with a steady-state dispersion (last 6 minutes of each RH step) below 0.8 %. The sensor also demonstrates reduced hysteresis when transitioning from increasing to decreasing humidity levels. Quantitatively, the hysteresis remains below 15 % of the full-scale output (FSO), confirming that the cellulose-acetate-coated IDE structure enables a reversible and stable dielectric response. The extracted Rp values remain above 100 kΩ up to 25 kHz for all humidity levels, confirming the predominantly capacitive behavior of the sensor in this frequency range and supporting the selection of 20 kHz as the operating frequency for Test #2.

Table 1 compares the humidity sensitivity of the sensors printed on the four polymer substrates. Sensitivity ($\Delta C_p/C_{p,RH = 20\,\%}$), defined as the fractional capacitance change with respect to the capacitance at the starting point (at RH = 20 %), increases with RH for all materials. The PP-based device exhibits the highest sensitivity at both 50 % and 80 % RH, whereas PVC and PE show comparable lower values, and PP-R lies between these two groups. These differences arise from substrate-dependent dielectric properties and surface morphology, which affect the field distribution and the effective permittivity experienced by the IDE structure. As typical for polymer-based capacitive humidity sensors, the response becomes nonlinear as RH approaches high values. Hysteresis and variability at the same RH condition are similar for all the samples.

TABLE I. SENSITIVITY OF THE PRINTED SENSORS ON DIFFERENT SUBSTRATES

	$\Delta C_p/C_{p,\,RH=20\,\%}$	
	RH=50 %	RH=80 %
Substrate	%	%
PE	1.12	4.48
PP	2.13	5.47
PP-R	1.04	4.35
PVC	0.92	4.31

Polymeric substrates do not significantly contribute to moisture absorption or desorption under the investigated conditions, and their effect can be considered negligible within the investigated humidity range. In all cases, the sensor response is negligible for relative-humidity changes between 20 % and 50 %, while characteristic response times of approximately 4 min are observed for humidity increases from 50 % to 80 % RH. During humidity decrease, longer recovery times are measured, on the order of 11 min for transitions from 80 % to 50 % RH and about 7 min for transitions from 50 % to 20 % RH.

A deeper investigation on the behavior of the PP-based sensors under repeated humidity cycling was evaluated in Test #2. Fig. 10 shows the normalized capacitance change $\Delta C_p/C_{p,\,RH = 20\,\%}$ as a function of relative humidity for three consecutive humidity cycles. In all cycles, the capacitance increases monotonically with humidity. The hysteresis observed during the first cycle is approximately 16 % of the full-scale output (FSO), decreasing to 11 %/FSO in the second cycle and 4 %/FSO in the third, indicating progressive stabilization of the CAB hygroscopic layer. Within the range 20–70 % RH, the sensor response exhibits high linearity, with coefficients of determination exceeding R-squared = 0.9921 for all cycles. Overall, the results of Test #2 confirm that the PP-based conformal sensor exhibits stable operation, fast conditioning, good linearity in the mid-RH range, diminishing hysteresis over consecutive cycles, and high repeatability, reinforcing its suitability for reliable humidity monitoring in real-world applications. In the same interval, the sensitivity during humidity increase varies between 0.0752 pF/%RH and 0.0798 pF/%RH, stabilizing at 0.0788 pF/%RH in the third cycle. During humidity decrease, the sensitivity is slightly lower, ranging from 0.064 pF/%RH to 0.070 pF/%RH, consistent with the observed hysteresis. Although nonlinearity increases for RH values above 80 %, the overall shape and amplitude of the response remain highly consistent across the three cycles. The repeatability, quantified as the maximum cycle-to-cycle deviation of the capacitance at the same imposed RH, is excellent. Even at 90 % RH, where hygroscopic materials typically show increased variability and the slope of the curve dramatically changes, the dispersion remains limited to 0.6 %, confirming the sensor's robustness under dynamic humidity conditions.

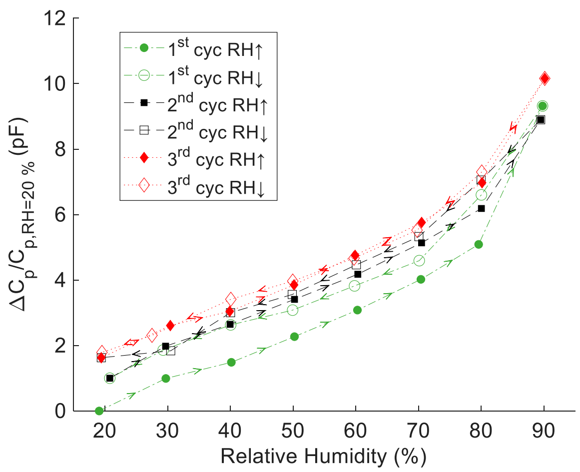

Fig. 10. Humidity response of the PP-based sensor during increasing and decreasing RH steps in Test #2.

V. CONCLUSIONS

This work demonstrates the feasibility of fabricating conformal capacitive humidity sensors directly onto non-planar automotive polymer tubes using Aerosol Jet Printing and photonic sintering. The proposed printing process enables the deposition of high-resolution silver IDE structures with good uniformity across substrates of different curvature and composition (PVC, PP, PE and PP-R), Although the experimental validation was performed on cylindrical tubes, the adopted fabrication method is broadly applicable to the wide range of non-planar polymer components commonly found in automotive interiors—such as door trims, pillar covers, dashboard structures, and molded housings—where localized moisture accumulation, condensation, or water ingress may occur. Because the printed sensor architecture is thin, lightweight, and inherently conformal, it can be integrated directly onto these surfaces without the need for additional packaging or mechanical fixtures. This enables distributed humidity monitoring in areas that are difficult to assess with conventional packaged sensors and supports early detection of infiltration and condensation phenomena that may compromise comfort, component integrity, or long-term reliability. Overall, the results confirm that printed, surface-conformal capacitive humidity sensors can be effectively implemented on typical automotive thermoplastics and represent a promising approach for embedding environmental-sensing functionality into complex, three-dimensional interior components. Future developments will focus on extending the conformal sensing approach to real non-planar automotive components, enabling integrated humidity monitoring wherever surface-mounted detection of condensation or moisture ingress is required.

ACKNOWLEDGMENT

The research activity reported in this paper was fully funded under the SMOFER project (Sistema di Monitoraggio e Fertilizzazione Robotizzata) through the disbursement of grants pursuant to the Ministerial Decree of 24 June 2022 – Fund for the Development of Artificial Intelligence, Blockchain and Internet of Things Technologies and Applications – University of Brescia – Project No. FTE0000341 – CUP: B87H22006390008 – COR: 22675808.

REFERENCES

[1] K. Gładyszewska-Fiedoruk and T. J. Teleszewski, “Modeling of Humidity in Passenger Cars Equipped with Mechanical Ventilation,” *Energies (Basel).*, vol. 13, no. 11, p. 2987, Jun. 2020, doi: 10.3390/en13112987.

[2] K. Alkaabi and M. Raza, “Revisiting the dynamics of car cabin environment and driver comfort,” *Front. Built Environ.*, vol. 8, Dec. 2022, doi: 10.3389/fbuil.2022.1041305.

[3] R. S. Kakade, “Cabin Air Humidity Model and its Application,” Apr. 2015. doi: 10.4271/2015-01-0369.

[4] A. N. Soloviev, I. A. Panfilov, O. N. Lesnyak, C. Y. J. Lee, and Y. M. Liu, “Numerical Simulation of Relative Humidity in a Vehicle Cabin,” 2023, pp. 515–527. doi: 10.1007/978-3-031-21572-8_45.

[5] A. Roman, B. Wu, B. Han, G. M. Reinacher, and S. G. Yousef, “Moisture Transport Through Housing Materials Enclosing Critical Automotive Electronics,” *IEEE Trans. Compon. Packaging Manuf. Technol.*, vol. 10, no. 4, pp. 541–550, Apr. 2020, doi: 10.1109/TCPMT.2020.2977111.

[6] H. Conseil-Gudla, G. Hamm, L. Muller, M. Hain, and R. Ambat, “Experimental Study of Moisture Ingress in First and Second Levels of Electronic Housings,” *IEEE Trans. Compon. Packaging Manuf. Technol.*, vol. 8, no. 11, pp. 1928–1937, Nov. 2018, doi: 10.1109/TCPMT.2018.2799233.

[7] S. Mola *et al.*, “Windshield Fogging Prevention by Means of Mean Radiant Temperature Sensor,” in *Advanced Microsystems for Automotive Applications 2004*, Berlin, Heidelberg: Springer Berlin Heidelberg, pp. 267–277. doi: 10.1007/978-3-540-76989-7_19.

[8] A. Ene and C. Teodosiu, “Studies dealing with defogging and de-icing phenomena on vehicles’ windshield: a review,” *IOP Conf. Ser. Earth Environ. Sci.*, vol. 664, no. 1, p. 012071, May 2021, doi: 10.1088/1755-1315/664/1/012071.

[9] F. Czerwinski, “Current Trends in Automotive Lightweighting Strategies and Materials,” *Materials*, vol. 14, no. 21, p. 6631, Nov. 2021, doi: 10.3390/ma14216631.

[10] J. Zikulnig, S. Lengger, L. Rauter, L. Neumaier, S. Carrara, and J. Kosel, “Sustainable Printed Chitosan-Based Humidity Sensor on Flexible Biocompatible Polymer Substrate,” *IEEE Sens. Lett.*, vol. 6, no. 12, 2022, doi: 10.1109/LSENS.2022.3224768.

[11] C. Fisher, L. N. Skolrood, K. Li, P. C. Joshi, and T. Aytug, “Aerosol-Jet Printed Sensors for Environmental, Safety, and Health Monitoring: A Review,” *Adv. Mater. Technol.*, vol. 8, no. 15, Aug. 2023, doi: 10.1002/admt.202300030.

[12] B. Arman Kuzubasoglu, “Recent Studies on the Humidity Sensor: A Mini Review,” *ACS Appl. Electron. Mater.*, vol. 4, no. 10, pp. 4797–4807, Oct. 2022, doi: 10.1021/acsaelm.2c00721.

[13] J. Boudaden *et al.*, “Polyimide-Based Capacitive Humidity Sensor,” *Sensors*, vol. 18, no. 5, p. 1516, May 2018, doi: 10.3390/s18051516.

[14] M. Chakraborty, A. Kalita, and K. Biswas, “PMMA-Coated Capacitive Type Soil Moisture Sensor: Design, Fabrication, and Testing,” *IEEE Trans. Instrum. Meas.*, vol. 68, no. 1, pp. 189–196, Jan. 2019, doi: 10.1109/TIM.2018.2838758.

[15] W. Yao, X. Chen, and J. Zhang, “A capacitive humidity sensor based on gold–PVA core–shell nanocomposites,” *Sens. Actuators B Chem.*, vol. 145, no. 1, pp. 327–333, Mar. 2010, doi: 10.1016/j.snb.2009.12.021.

[16] J. J. Steele, M. T. Taschuk, and M. J. Brett, “Nanostructured Metal Oxide Thin Films for Humidity Sensors,” *IEEE Sens. J.*, vol. 8, no. 8, pp. 1422–1429, Aug. 2008, doi: 10.1109/JSEN.2008.920715.

[17] T. Islam, L. Kumar, and S. A. Khan, “A novel sol–gel thin film porous alumina based capacitive sensor for measuring trace moisture in the range of 2.5–25ppm,” *Sens. Actuators B Chem.*, vol. 173, pp. 377–384, Oct. 2012, doi: 10.1016/j.snb.2012.07.014.

[18] S. Yao, Q. Zhang, W. Ding, Y. Zhang, J. Zhang, and C. Wang, “Capacitive humidity sensors based on PVA/CAB compound film with potassium acetate-enhanced sensitivity,” in *2022 15th International Congress on Image and Signal Processing, BioMedical Engineering and Informatics (CISP-BMEI)*, IEEE, Nov. 2022, pp. 1–5. doi: 10.1109/CISP-BMEI56279.2022.9979920.

[19] V. Ducéré, A. Bernès, and C. Lacabanne, “A capacitive humidity sensor using cross-linked cellulose acetate butyrate,” *Sens. Actuators B Chem.*, vol. 106, no. 1, pp. 331–334, Apr. 2005, doi: 10.1016/j.snb.2004.08.028.